Physical and mechanical properties of low, ultralow and no cement refractory castables containing MgO nanoparticles developed *in situ* by means of polymeric resins

(Propriedades físicas e mecânicas de concretos refratários de baixo, ultrabaixo e sem cimento contendo nanopartículas de MgO desenvolvidas in situ por meio de resinas poliméricas)

J. A. Alves Júnior[1]*, J. B. Baldo[1]
[1]*Federal University of São Carlos, Department of Materials Engineering,
Rod. Washington Luiz, km 235, 13565-905, S. Carlos, SP, Brazil*

Abstract

The introduction of MgO nanoparticles developed *in situ* in the matrix of high-alumina low cement, ultra-low and no cement refractory castables was made by means of a low viscosity containing aqueous polymeric resin, produced by the Pechini method. The addition of the liquid resin to the castables played two roles: first to serve as a supplier of mixing water and second as a precursor of nanoparticles of MgO, which were formed *in situ* in the castables matrices during firing. The results confirmed the benefits brought by the developed *in situ* MgO nanoparticles on the refractory properties of the investigated castables.
Keywords: refractory castables, polymeric resins, MgO nanoparticles, Pechini method.

Resumo

A introdução de nanopartículas de MgO desenvolvidas in situ na matriz de concretos refratários de baixo teor de cimento, ultrabaixo e sem cimento foi feita por meio de uma resina polimérica aquosa de baixa viscosidade, produzida pelo método Pechini. A adição da resina líquida aos concretos desempenhou dois papéis: primeiro serviu como fornecedor de água de mistura e segundo como precursor de nanopartículas de MgO, que foram formadas in situ nas matrizes de concretos durante a queima. Os resultados confirmaram os benefícios trazidos pelas nanopartículas de MgO desenvolvidas in situ nas propriedades refratárias dos concretos investigados.
Palavras-chave: concretos refratários, resinas poliméricas, nanopartículas de MgO, método Pechini.

INTRODUCTION

A substantial increase in the performance of refractory castables has been obtained in the last three decades by reducing the content of calcium aluminate cement (CAC), in the range from 2 to 6 wt% or even its virtual absence in refractory castables. As a consequence, because of the resulting lower CaO contents in these castables matrices, a strong reduction in the amount of eventual liquid-phase development at high temperature could be achieved. In the search for refractory castables without cement for more demanding applications, the 'no cement' variety was developed using hydratable alumina, colloidal silica or colloidal alumina as binding agents. Therefore, the modern refractory castables are able to present creep and corrosion resistance similar to formed refractories of the same class [1, 2]. The advantage of using the hydratable alumina

as a binder is that it does not need to be cured under high relative humidity. When hydratable alumina reacts with water, it forms a thick layer of pseudoboehmite gel around the aggregates during the hydration process. Part of this gel is then transformed into boehmite ($Al_2O_3.2H_2O$) and crystalline bayerite ($Al_2O_3.3H_2O$) [3, 4].

Aiming to obtain an overall improvement of properties, recently there has been a great interest in including nanoparticles of highly refractory oxides in ceramics. The introduction of nanoparticles of refractory oxides in the matrix of advanced refractory castables can be considered a new route to improve physical and thermo-mechanical properties of these materials. Until now, the refractory oxide nanoparticles were generally added to castables either in powder form, or as colloidal suspensions of silica or alumina [5, 6]. However, the use of the colloidal silica carries SiO_2 to the castable matrix, forming low melting compounds other than mullite. In addition, the presence of silica is not desirable for several steelmaking processes. On the other hand, the use of colloidal alumina has some drawbacks such

**jjunior8404@gmail.com*
https://orcid.org/0000-0001-9903-0506

as not enough solid contents to provide strength and the need for drying over 50 °C to set and harden.

In order to take advantage of the potential of nanoparticles, an innovative way of introducing nanoparticles of refractory oxides in castables was developed by the present authors. It consists of forming *in situ*, during firing, nanoparticles of highly refractory oxides (Al_2O_3, MgO, Cr_2O_3, ZrO_2) in the castables matrices. Through this novel technique, aqueous Pechini resins containing Al^{3+}, Mg^{2+}, Cr^{3+} and Zr^{4+} cations in their polymeric chains are introduced playing the double role of water vehicle for workability and hydration, while at the same time fulfilling the role of precursor for *in situ* development of the targeted refractory oxides nanoparticles [7-9]. Through this new route, agglomeration problems of nanoparticle additions in powder form are eliminated. Moreover, the nanoparticles are developed in a nascent state closely adhered to the aggregates, being much more reactive than when colloidal particles or ready-made nanoparticles in powder form are introduced. In this way, there is a great improvement in overall properties of refractory castables. In the present study the *in situ* development of MgO nanoparticles is shown together with the benefits coming from its reaction with fine alumina aggregates, leading also to the *in situ* formation of magnesium aluminate spinel ($MgAl_2O_4$) and hebonite ($CaO.6Al_2O_3$), chemically stable and neutral refractory compounds. When the spinel and hebonite phases form *in situ*, they occur with expansion, helping the closure of cracks increasing the resistance to slag attack and metal penetration [10-13].

EXPERIMENTAL PROCEDURE

Preparation of the Mg resin using the Pechini method: in 1 L of water (under stirring), 250.3 g of citric acid was added. After complete dissolution, 102.4 g of magnesium nitrate hexahydrate were added slowly. The solution remained several hours under agitation until complete dissolution of the magnesium nitrate hexahydrate. Then the solution was heated to 70 °C and remained for 1 h at this temperature. After this time, 48.6 mL of ethylene glycol was added and the solution was heated to 90 °C, remaining at this temperature for 2 h. When added to the castable, the mixture was left stirring for 2 min [6]. In this study, an attenuated Mg resin was prepared using the reagents shown in Table I. The aqueous resin presented a viscosity of 7 cP. In order to check the formation of the MgO nanoparticles, X-ray diffraction (XRD) and BET analyses were done after a separate test of pyrolysis and burning of the Mg aqueous resin. The crystallite size was determined by the association of the XRD technique with the Scherrer method shown by:

$$T = K.\lambda/(\beta.\cos\theta) \tag{A}$$

where T is crystallite size, K constant, λ X-ray wavelength, β broadening at half maximum intensity, and θ Bragg angle.

Castable specimen preparation: specimens with dimensions of 120x25x25 mm of low cement (LCC), ultra-low cement (ULCC) and no cement (NCC) castable types, using water or Mg^{2+} resin as the mixing liquid, were produced by mixing in a 5 L capacity planetary mixer (mod. 020, Amadio) and molded in metallic molds under light vibration in a vibration table NTG-1220N for 20 s under a 2 mm amplitude. In Table II the raw materials used, as well as their respective percentage for each of the three types of castables, are shown. The compositions were formulated aiming the optimization of particle packing, using Andreasen's particle packing procedure under a distribution modulus of q=0.26 [14, 15]. The castables LCC$_{water}$, ULCC$_{water}$, and NCC$_{water}$ were molded with 5.8 wt% water. The castables LCC$_{MgO}$, ULCC$_{MgO}$, and NCC$_{MgO}$ were molded with 8 wt% of the liquid Mg polymeric resin. After 24 h, the specimens were demolded and dried for 24 h at 110 °C, after which they were fired at 1450 °C/2 h in an EDG-1700 electric muffle.

Physical and thermo-mechanical testing: apparent density and apparent porosity were evaluated by the Archimedes principle, using samples from the broken pieces of the fired bar-shaped specimens after being submitted to three-point bend flexure strength measurement in a universal testing machine (DL10000-100 kN$_{max}$, Emic)

Table I - Reagents used to produce the Mg^{2+} polymeric resin.
[Tabela I - Reagentes utilizados na produção da resina polimérica de Mg^{2+}.]

Reagent	Formula
Citric acid monohydrate (Merck Millipore)	$C_6H_8O_7.H_2O$
Magnesium nitrate hexahydrate (Merck Millipore)	$Mg(NO_3)_2.6H_2O$
Ethylene glycol (Synth)	$C_6H_6O_2$

Table II - Compositions (wt%) of the three different castables.
[Tabela II - Composição (% em massa) dos três diferentes concretos.]

Raw material	FA 4/10	FA 10/20	FA 20/40	FA 70/140	FA #325	CA CT3000	CAC	HA	MS 971-U	STP	APA
LCC	21.0	16.0	10.0	13.0	17.0	13.0	5.0	-	5.0	0.1	0.05
ULCC	21.0	16.0	10.0	13.0	18.0	14.5	2.5	-	5.0	0.1	0.05
NCC	21.0	16.0	10.0	13.0	18.0	13.0	0.5	3.5	5.0	0.1	0.05

FA - Elfusa AL fused alumina (99.47% Al_2O_3, 0.04% Fe_2O_3); CA - Almatis CL-370 calcined alumina (99.7% Al_2O_3, 0.05% Fe_2O_3, 0.07% SiO_2); CAC - Kerneos Secar 71 calcium aluminate cement (>68.5% Al_2O_3, <31.0% CaO, <0.8% SiO_2, <0.4% Fe_2O_3); HA - Almatis Alphabond 300 hydratable alumina; MS - Elkem 971U microsilica (>90% SiO_2, <1% H_2O); STP - Merck Millipore 85% sodium tripolyphosphate; APA - Dyspersal B130 ammonium polyacrylate 44%.

using a 120 mm span and a crosshead speed of 1 mm/min. Dynamic elastic modulus measurement by the impulse excitation technique (IET) is a valuable tool in revealing how the microstructure evolves during heating and cooling. Using IET, the dynamic elastic modulus (DEM) of the bar-shaped fired specimens was evaluated in a heating/cooling cycle from room temperature to 1500 ºC and back, under a heating rate of 5 ºC/min and a cooling rate of 10 ºC/min. The DEM was determined using a RFDA HT 1600 from IMCE, Belgium. The thermal expansion behavior of the different castables was also evaluated from room temperature to 1300 ºC, in a dilatometer coupled to the RFDA HT-1600 equipment, under a heating rate of 5 ºC/min. The thermal shock resistance of the different castables was evaluated using the residual flexural strength after submitting the fired (1450 ºC/2 h) bar-shaped specimens to one cycle exposure at sudden temperature gradients of ΔT= 300-600-900 ºC in running water at 24 ºC.

Scanning electron microscopy analysis: was performed to analyze the microstructure of the castables with and without the use of the polymer resin. The castables were cut in the shape of 10 mm cubes and later had their surfaces polished. The analyses were performed in an FEI Inspect S50. *Phase assembly by XRD analysis*: the resulting mineralogical compositions of the castables were determined by X-ray diffraction analysis, using Bruker D-8 Advanced ECO.

RESULTS AND DISCUSSION

Characteristics of the resulting MgO nanopowder: it was seen that after pyrolysis and firing of the Mg^{2+} polymeric resin, the development of pure crystalline MgO indeed occurred already at 600 ºC, increasing strongly its crystalline character at 1000 ºC as shown by the X-ray diffractograms presented in Fig. 1. The results of surface area and crystallite size (calculated by Scherrer equation) are shown in Table III. It was clear that the resulting powder after pyrolysis and firing (1000 ºC/1 h) of the Mg polymeric resin was really nanometric.

Results of physical properties: it is known that the apparent porosity directly influences the mechanical properties such
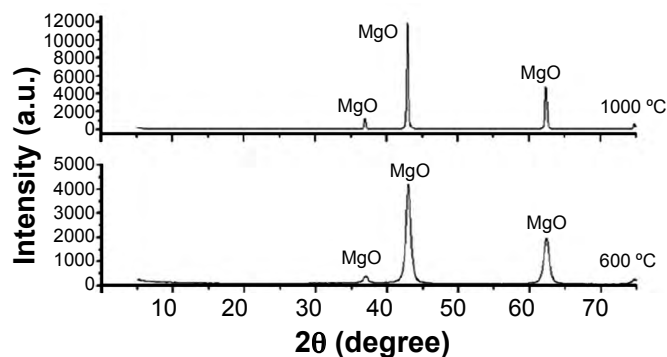
Table III - Particle size, surface area and crystallite size of MgO after pyrolysis and firing (1000 ºC/1 h) of the Mg^{2+} polymeric aqueous resin.
[Tabela III - Tamanho de partícula, área superficial e tamanho de cristalito do MgO após pirólise e queima (1000 ºC/1 h) da resina polimérica de Mg^{2+}.]

Surface area - BET (m^2/g)	Particle size (nm)	Crystallite size (nm)
83.1	21	18

as modulus of elasticity and mechanical strength of ceramic materials [14]. In Table IV it is shown the results of apparent porosities and densities of the investigated castables, after firing at 1450 ºC/2 h. It was noted that the concretes molded with the Mg resin presented lower apparent porosity and higher densification than those molded with water. This fact indicated that the *in situ* generation of nanoparticles led to improved densification, contradicting the expected potential negative effect of the increase of pore volume fraction, as a result of the pyrolysis of the resin, releasing CO_2 and the vaporization of part of its aqueous content. The densification effect of MgO nanoparticles found in this study was in line with the literature [16], which found the same densifying effect after adding submicron-sized spinel to high-alumina refractory castables.

Results of scanning electron microscopy (SEM): through the SEM micrographs presented in Fig. 2, it was possible to verify, as already expected from the results of physical properties, that the specimens without the presence of the resin presented a less compact microstructure with a higher quantity of pores when compared to the specimens with the presence of the resin. The observed compact microstructure of the castable molded with the Mg resin was comparable to the results presented in [16]. We may consider that this fact was directly responsible for the improvement of the mechanical properties of castables [14], which is shown in the mechanical property results.

Results of X-ray diffraction: XRD testing was used in order to evaluate comparatively the resultant phase assembly of the different castables (with and without the

Figure 1: X-ray diffraction pattern of powder resulting from the pyrolysis and firing of the Mg^{2+} polymeric aqueous resin.
[Figura 1: Difratograma de raios X do pó resultante da pirólise e queima da resina polimérica de Mg^{2+}.]

Table IV - Results of apparent porosity and density of the investigated castables after firing at 1450 ºC/2 h.
[Tabela IV - Resultados de porosidade e densidade aparentes dos concretos investigados após queima a 1450 ºC/2 h.]

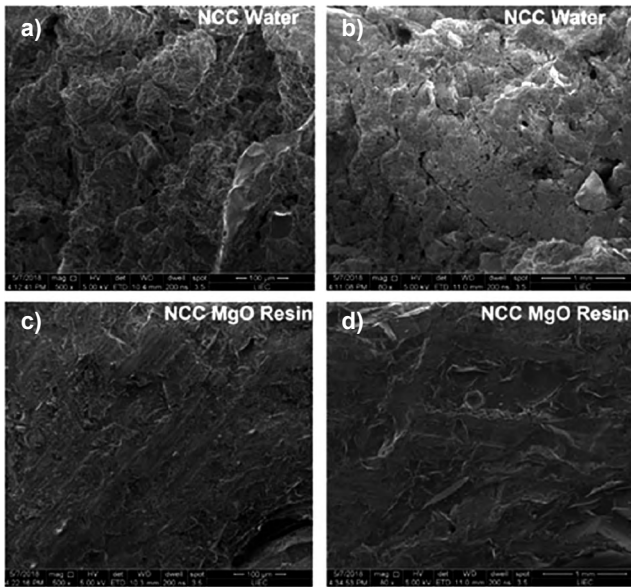| Castable	Apparent density (g/cm^3)	Apparent porosity (%)
LCC_{water}	3.02	21
$ULCC_{water}$	2.91	21
NCC_{water}	2.85	19
LCC_{MgO}	3.07	19
$ULCC_{MgO}$	3.16	19
NCC_{MgO}	3.29	16

Figure 2: Scanning electron micrographs of the polished surface after firing at 1450 ºC/2 h of the castables molded with and without the Mg resin.
[Figura 2: Micrografias eletrônicas de varredura da superfície polida após queima a 1450 °C/2 h dos concretos moldados com e sem a resina de Mg.]

Mg resin), after firing at 1450 ºC/2h. A comparison between the Figs. 3a and 3b indicated that the main mineralogical composition differences between the LCC_{water} and LCC_{MgO} castables were: a) presence of spinel ($MgAl_2O_4$) in the LCC_{MgO} castable; b) absence of spinel ($MgAl_2O_4$) in the LCC_{water}; and c) more mullite ($3Al_2O_3.2SiO_2$) and hebonite ($CaO.6Al_2O_3$ - CA_6) and less gehlenite ($2CaO.Al_2O_3.SiO_2$)

were developed in the LCC_{MgO} castable. From the intensity of the spinel peaks, it may be inferred that all the MgO coming from the Mg resin upon firing was transformed into spinel after reacting with fine alumina from the aggregates. This was so because when 8 wt% of liquid resin was transformed into MgO nanoparticles, after its pyrolysis and firing, it resulted in only 0.7 wt% of MgO in the whole castable mix. The presence of gehlenite in LCC_{water} resulted from the reaction of CaO coming from the calcium aluminate cement with microsilica and alumina fines in the castable matrix. Apparently, the presence of MgO inhibited a more intensive development of gehlenite. This may enhance indirectly the hot modulus of rupture as shown by the values of dynamic elastic modulus. For the NCC castables, the virtual absence of gehlenite ($2CaO.Al_2O_3.SiO_2$) as shown in Figs. 3c and 3d led us to infer that all the CaO coming from the 0.5 wt% calcium aluminate cement used in both NCC_{water} (Fig. 3c) and NCC_{MgO} (Fig. 3d) castables reacted only with the alumina fines forming CA_6. On the other hand, all the silica content coming from the 5 wt% microsilica used in both castables reacted with alumina fines forming mullite. In this case it appeared that the Mg resin favored mullite and CA_6 formation. These findings agreed well with what was found in [17]. The phases CA_6, spinel, and gehlenite identified by XRD analysis indicated that the castables molded with the resin can display good resistance to the thermal shock [14, 16-19] as it is shown ahead.

Results of cold mechanical strength using the 3-point bending test: from the results presented in Fig. 4, it is apparent that the resin incorporated in the refractory castables turned their respective flexural strengths substantially higher (>75%) than the ones molded with water. The use of MgO
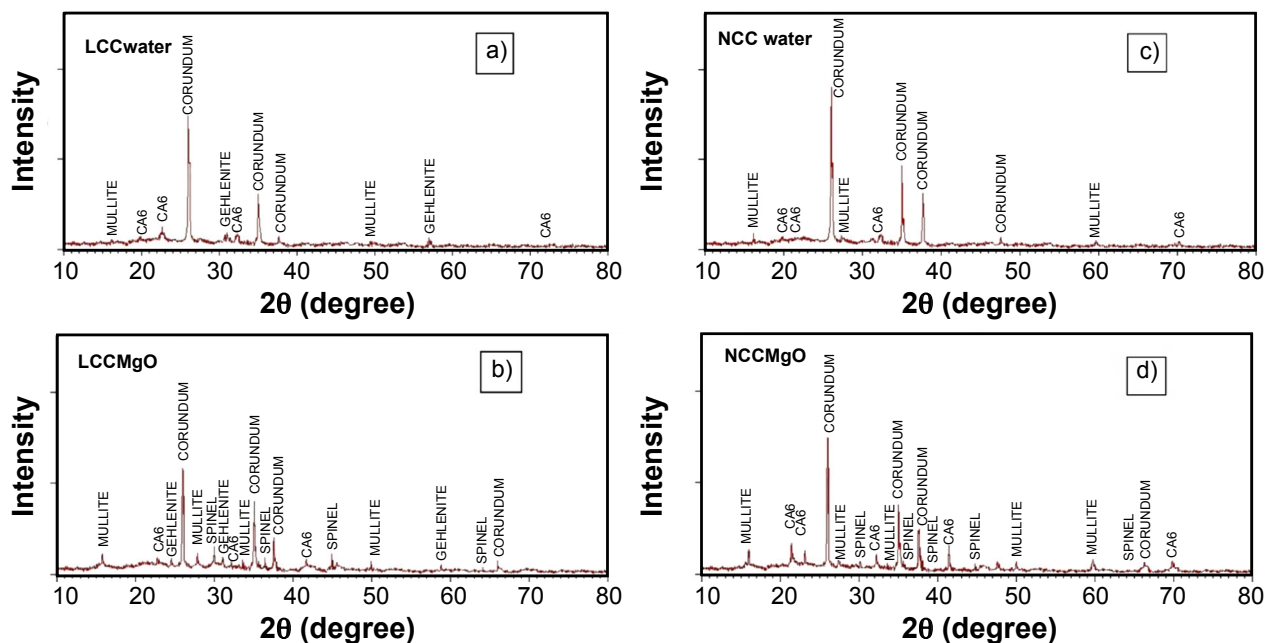

Figure 3: X-ray diffraction patterns of castables after firing at 1450 ºC/2 h: a) LCC_{water}; b) LCC_{MgO}; c) NCC_{water}; and d) NCC_{MgO}.
[Figura 3: Difratogramas de raios X dos concretos após queima a 1450 °C/2 h: a) baixo teor de cimento moldado com água; b) baixo teor de cimento moldado com a resina de MgO; c) sem cimento moldado com água; e d) sem cimento moldado com a resina de MgO.]
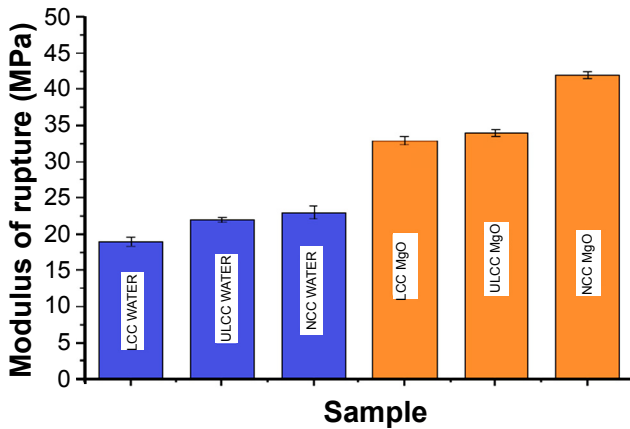
Figure 4: Room temperature modulus of rupture in 3-point bending of the investigated castables after firing at 1450 ºC/2 h. Values are the average of 5 tested specimens for each castable.
[Figura 4: Módulo de ruptura (em três pontos) à temperatura ambiente dos concretos estudados após queima a 1450 °C/2 h. Valores são médias de 5 espécies de cada concreto.]

resin as an aqueous vehicle and nanoparticle precursor, combined with the replacement of calcium aluminate cement by hydratable alumina, caused a significant increase in the strength as shown by the NCC_{MgO} castable. These facts may be credit to an enhancement of the sintering during firing caused by the high reactivity of the *in situ* formed MgO nanoparticles with the fine alumina aggregates, forming magnesium aluminate spinel and favoring the development of the CA_6 phase in an interlocking mode, strongly bridging the alumina aggregates, as was reported in [16]. In addition, the spinel phase development occurred with expansion, leading to a closure of pores causing an indirect increase in the strength. This also happened for the CA_6 phase. The high levels of three-point bend strength (>32 MPa) achieved by the castables molded with the liquid Mg resin after firing at 1450 ºC/2 h were considerably higher than the values reported in the literature (even the ones after firing at 1600 ºC/3 h), when spinel phase is added ready-made or developed *in situ* in refractory castables by the reaction of added MgO powder and the fine alumina aggregate [7, 11-13, 16, 20].

Results of thermal expansion behavior: in Fig. 5, the thermal expansion behavior of the investigated castables is presented. Through Fig. 5a it can be seen that the final expansions of the castables molded with water followed the ranking: $NCC_{water} < ULCC_{water} < LCC_{water}$. In addition, the thermal expansion coefficients [$\alpha = (dL/L).(1/\Delta T)$] from room temperature to 600 ºC were almost the same ($\alpha \approx 8.1 \times 10^{-6}$ ºC^{-1}) for the three castables. However, LCC_{water} presented a higher value ($\alpha \approx 8.7 \times 10^{-6}$ ºC^{-1}) from 600 ºC. These data were compatible with no addition calcium aluminate bonded high-alumina (>85% Al_2O_3) containing refractories. In addition, they started to display a kind of softening (creeping) around 750 ºC. In Fig. 5b a similar trend presented by the thermal expansion behavior of the castables molded with the Mg polymeric resin can be seen. The same ranking with respect to dimensional changes variations was maintained, that is
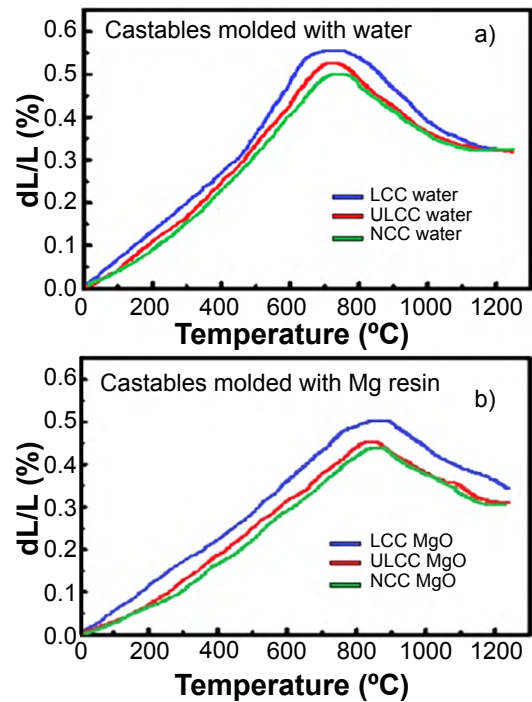

Figure 5: Linear dimensional variation (dL/L) of the different castables specimens molded with 5.8 wt% water (a) and 8 wt% Mg aqueous polymeric resin (b), after firing at 1450 ºC/2 h.
[Figura 5: Variação linear dimensional (dL/L) dos espécimes de diferentes concretos moldados com 5,8% de água (a) e 8% da resina polimérica de Mg (b), após queima a 1450 °C/2 h.]

$NCC_{MgO} < ULCC_{MgO} < LCC_{MgO}$. The main difference presented by the castables molded with Mg resin was that their final expansion values were at least 20% smaller than the ones molded with water. The same occurred for their thermal expansion coefficients ($\alpha \approx 6.5 \times 10^{-6}$ ºC^{-1}) comparatively to the castables molded with water. In addition, their softening started to occur at approximately 900 ºC, while for the castables molded with water the softening started at 750 ºC. These important differences brought by the inclusion of MgO can be credit to the development of magnesium aluminate spinel and CA_6 (which have smaller thermal expansion coefficients than alumina), as a consequence of the reaction between the fine alumina aggregates with the developed MgO nanoparticles and CaO coming from the calcium aluminate cement [17].

Results of dynamic elastic modulus measurements: the development of dynamic elastic modulus has been used as a tool to understand the dynamic evolution of refractory microstructures [21, 22]. In Fig. 6 the results of elastic modulus versus temperature using the IET technique are presented. It was seen the following features: a) the magnitude of dynamic elastic modulus (DEM) of all the castables molded with the Mg resin was substantially higher than the ones corresponding to the castables molded with water; the magnitude of the resulting final DEM values at room temperature, are expressively higher than the ones reported in the literature for the high-alumina castables [16, 23]; b) for all castables independent of the liquid vehicle
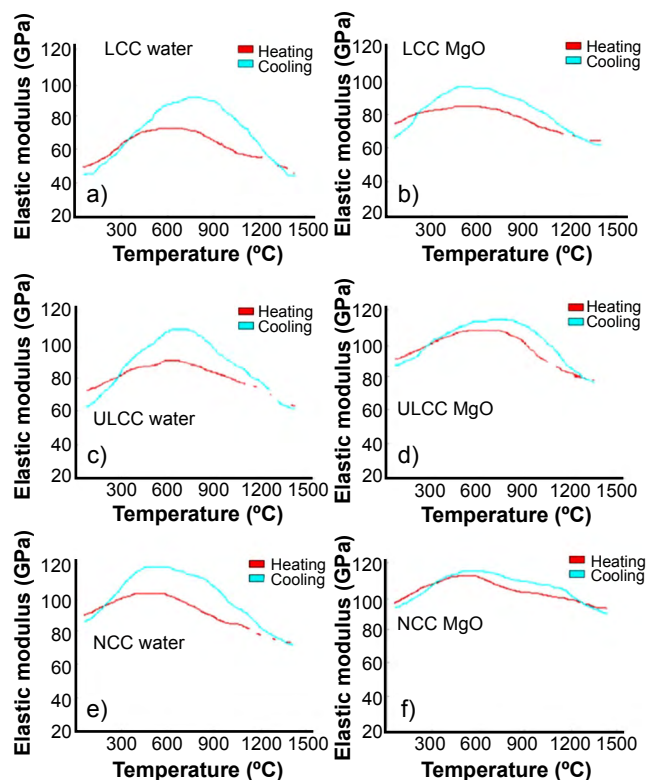
Figure 6: Dynamic elastic modulus measurements using IET of dried (110 ºC/12 h) bars of the investigated castables, with a heating rate of 5 ºC/min until 1500 ºC and a cooling rate of 10 ºC/min.
[Figura 6: Medidas do módulo elástico dinâmico usando a técnica de excitação por impulso de corpos de prova secos (110 °C/12 h) com taxa de aquecimento de 5 °C/min até 1500 °C e taxa de resfriamento de 10 °C/min.]

used in their molding (water or Mg resin), there was a clear trend showing that the decrease in the calcium aluminate content of the castable led to an increase in the dynamic elastic modulus value, making an apparent DEM ranking of $E_{LCC}<E_{ULCC}<E_{NCC}$; c) for all castables molded with water during the heating branch, there was an errant loss of signal (damping) for temperatures higher than 1200 ºC; the damping may be related to the liquid phase development and/or pyroplasticity; in addition, DEM values after cooling to room temperature were always smaller than their initial value at the starting of the heating branch because some microstructure damage; d) it was also seen that there was a mismatch between the heating and cooling branches, creating a visible hysteresis area which was more pronounced for the castables molded with water. The hysteresis phenomenon can be credited to microstructure stability features. Considering that refractory castables are the monolithic type, they present dynamic behavior achieving microstructure stability only as a function of temperature and time. In this sense, it was seen that the castables molded with the Mg liquid resin, by displaying smaller hysteresis areas, presented a higher maturation degree ending up to be more stable than the ones molded with water. As far as the authors' knowledge, there are no reports in the literature showing results of DEM during heating and cooling of high-alumina refractory
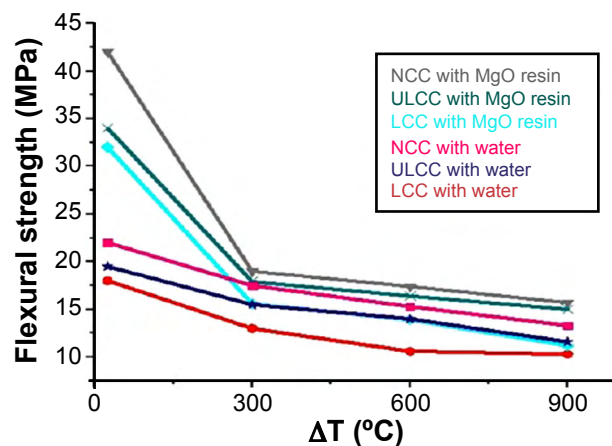

Figure 7: Residual flexural strength after a single thermal shock under sudden temperature gradients of ΔT= 25 (without thermal shock), 300, 600 and 900 °C.
[Figura 7: Resistência à flexão em três pontos após um ciclo de choque térmico nos gradientes de temperatura de 25 (sem choque térmico), 300, 600 e 900 ºC.]

castables containing nanoparticles.

Thermal shock results: in Fig. 7 the results of thermal shock relative to the six castables are shown. Considering the strong decrease in flexural strength, it was seen that a ΔT=300 ºC was critical for all the castables, causing a ~30% decrease in the original flexural strength without thermal shock for the castables molded with water. Conversely, it was clear that the same ΔT=300 ºC was more critical for the castables molded with the Mg resin, causing a ~50% decrease in the original strength without thermal shock. Based on the magnitude of the flexure strength decay of the castables molded with the Mg resin, we may infer a resulting high degree of microstructure damage in them. However, their ΔT=300 ºC flexural strength decay did not impair the load-bearing ability of these castables, which were still stronger (except LCC$_{MgO}$) than the ones molded with water. An interesting point noticed was that, after the critical ΔT=300 ºC, the strength decay almost leveled off for castables of ultralow and no cement type molded with Mg resin. This fact, indirectly implied good microstructure stability (stopping crack growth) under increased severity of thermal shock, keeping high strength levels. The presence of the CA$_6$ and spinel phases as already mentioned also directly influenced the high resistance to thermal shock in the castables molded with resin. Similar results with addition of spinel particles of different granulometry were obtained in castables and in spinel composites [16, 19, 20, 24].

CONCLUSIONS

A comprehensive analysis of the obtained results led to the conclusion that the use of a novel technique for the *in situ* development of MgO nanoparticles within the matrix of LCC, ULCC and NCC refractory castables using a Mg polymeric aqueous resin provided a strong increase in the physical and mechanical properties, with a low overall

thermal expansion, at the same time aiding the formation of highly refractory phases ($MgAl_2O_4$, $CaO.6Al_2O_3$, $3Al_2O_3.2SiO_2$) while inhibited the formation of low melting point phases as, for example, gehlenite ($2CaO.Al_2O_3.SiO_2$).

ACKNOWLEDGMENTS

REFERENCES

[1] C. Parr, R. Roesky, CN Refract. **5**, 6 (2001) 6.
[2] F.I. Tomsu, S. Palco, Int. Ceram. Rev. **3**, 4 (2011) 202.
[3] T.A. Bier, E.N. Bunt, C. Parr, in Latin-Am. Ass. Refract. Manuf. Meet., ALAFAR, Buenos Aires (1996) 75.
[4] W.E. Lee, W. Vieira, S. Zhang, K.G. Ahari, H. Sarpoolaky, C. Parr, Int. Mater. Rev. **46**, 3 (2001) 145.
[5] M. Nouri-Khezrabad, M.A. Braulio, V.C. Pandolfelli, F. Golestani-Fard, Ceram. Int. **39**, 4 (2013) 3479.
[6] J. Roy, S. Chandra, S. Maitra, Ceram. Int. **45**, 1 (2019) 19.
[7] S. Mukhopadhyaya, P.K. Daspoddar, Mater. Manuf. Process. **21**, 3 (2006) 669.
[8] J.B. Baldo, E.L. da Silva, J.A. Alves Jr., "Advanced refractory castables containing nanoparticles of oxides produced by the Pechini method", Patent Appl., submitted Braz. Patent Office (2019).
[9] M.P. Pechini, "Method of preparing lead and alkaline earth titanates and niobates and coating method using the same to form a capacitor", US Patent 3330697 (1967).
[10] M. Schnabel, A. Buhr, R. Exenberger, C. Rampitsch, WorldForum **2**, 2 (2010) 87.
[11] A.K. Sing, R. Sarkar, Ceram. Int. **42**, 15 (2016) 17410.
[12] L. Nevřivová, Mater. Sci. Forum **908** (2017) 139.
[13] S. Otroj, A. Daghighi, Ceram. Int. **37** (2011) 1003.
[14] H.N. Yoshimura, A.L. Molisani, G.R. Siqueira, A.C. de Camargo, N.E. Narita, P.F. Cesar, H. Goldenstein, Cerâmica **51**, 319 (2005) 239.
[15] J.E. Funk, D.R. Dinger, Int. Ceram. Rev. **43**, 5 (1994) 50.
[16] P. Chen, Y. Wang, X. Li, B. Zhu, Int. J. App. Ceram. Technol. **14** (2017) 748.
[17] E.C. Sako, M.A.L.E. Zinngreb, S.R. Van der Laan, V.C. Pandolfelli, J. Am. Ceram. Soc. **95**, 5 (2012) 1732.
[18] D. Milanez, E.Y. Sako, M.F. Maia, M.A.L. Braulio, L.R.M. Bittencourt, V.C. Pandolfelli, Cerâmica **56**, 337 (2010) 91.
[19] G.B. Cintra, M.A.L. Braulio, M.A.M. Brito, L.R.M. Bittencourt, V.C. Pandolfelli, Cerâmica **54**, 331 (2008) 287.
[20] C. Aksel, E. Riley, J. Eur. Ceram. Soc. **23** (2003) 3079.
[21] J. Werner, C.G. Aneziris, S. Schafoner, J. Fruhstorfer, M. Oppelt, S. Dudczig, in 56th Int. Colloq. Refract., Refract. Ind. (2013) 138.
[22] A.K. Swarnakaras, S. Gimenez, S. Salehic, J. Vleugelsd, O. van der Beieste, Key Eng. Mater. **333** (2007) 235.
[23] F. Simonin, C. Olagnon, S. Maximilien, G. Fantozzi, J. Am. Ceram. Soc. **83**, 10 (2000) 781.
[24] W. Qiu, G. Ruan, J. Ouyang, Y. Zhao, Int. J. Appl. Ceram. Technol. **11**, 6 (2014) 993.